Cellular Microbiology (2011) **13**(1), 81–91
doi:10.1111/j.1462-5822.2010.01521.x
First published online 16 September 2010

A combined luciferase imaging and reverse transcription polymerase chain reaction assay for the study of *Leishmania* amastigote burden and correlated mouse tissue transcript fluctuations

Emilie de La Llave, Hervé Lecoeur, Aurore Besse, Geneviève Milon, Eric Prina† and Thierry Lang*†
Institut Pasteur, Département de Parasitologie et Mycologie, Immunophysiologie et parasitisme intracellulaire, 25 rue du Dr Roux, 75724 Paris cedex15, France.

Summary

Laboratory mice display features of *bona fide* hosts for parasites such as *Leishmania major* and *Leishmania donovani*. Characterizing the amastigote population size fluctuations and the mouse transcript abundance accounting for these fluctuations demands the capacity to record in real time and integrate quantitative multiparametric datasets from the host tissues where these processes occur. To this end, two technologies, luciferase-expressing *Leishmania* imaging and a very sensitive quantitative analysis of both *Leishmania* and mouse transcripts, were combined. After the inoculation of either *L. major* or *L. donovani*, the amastigote population size fluctuations – increase, plateau and reduction – were monitored by bioluminescence. It allowed a limited number of mice to be selected for further analysis of both mouse and amastigote transcripts using the real-time quantitative polymerase chain reaction assay we set up. The illustrative examples displayed in the present analysis highlight a correlation between the transcriptional signatures displayed by mouse tissues with the amastigote burden fluctuations. We argue that these two combined technologies will have the potential to provide further insights on complex phenotypes driven by *Leishmania* developmental programs in the tissues of the mammal hosts.

Received 26 May, 2010; revised 30 July, 2010; accepted 18 August, 2010. *For correspondence. E-mail thierry.lang@pasteur.fr; Tel. +33 1 45 68 86 73; Fax +33 1 45 68 83 32.
†Both authors contributed equally.

Introduction

Leishmania major and *Leishmania donovani* were initially detected as etiological agents of human localized cutaneous leishmaniasis (LCL) and visceral leishmaniasis (VL) respectively (Murray *et al*., 2005; Banuls *et al*., 2007). We now know that LCL reflects transient localized skin lesions, whereas VL reflects systemic skin-distant damages that take place in organs such as the liver, the spleen and bone marrow. To decipher and characterize the dynamics of these *Leishmania*-driven processes in human and non-human *Leishmania*-hosting populations, different models based on laboratory rodents have been developed (Kaye *et al*., 2004; Scott, 2005; Kimblin *et al*., 2008; Peters *et al*., 2008; Sakthianandeswaren *et al*., 2009; Sacks and Noben-Trauth, 2002). Until now, in mammals, the analysis of parasite burden fluctuations and host immune responses were performed on tissue samples collected from sacrificed laboratory rodents (Murphy *et al*., 1998; Alexander *et al*., 2000; Belkaid *et al*., 2000; 2002; Nicolas *et al*., 2002). Though informative, these approaches have various drawbacks including the sacrifice of numerous laboratory rodents and the requirement of a large number of time-point analyses, obstacles that have prevented researchers from accurately delineating and characterizing *Leishmania*-driven processes.

Recently, laboratory mice have been recognized as model mammals displaying features of *bona fide* hosts, at least for the two *Leishmania* species introduced above. Moreover, genetically modified *L. major* parasites that stably express a reporter luciferase molecule have been shown to be valuable tools to monitor, in real time, the *Leishmania* amastigote burden at the level of the skin inoculation site (Lang *et al*., 2005; 2009). Thus, the capacity to record in real time and to integrate quantitative multiparametric datasets from mammalian tissues is of utmost importance to unveil and characterize the dynamic biological processes that account for *Leishmania* perpetuation. The present study shows how the combination of two technologies, luciferase-expressing *Leishmania* imaging and quantitative analysis of both *Leishmania* and mouse transcripts, allows us to achieve

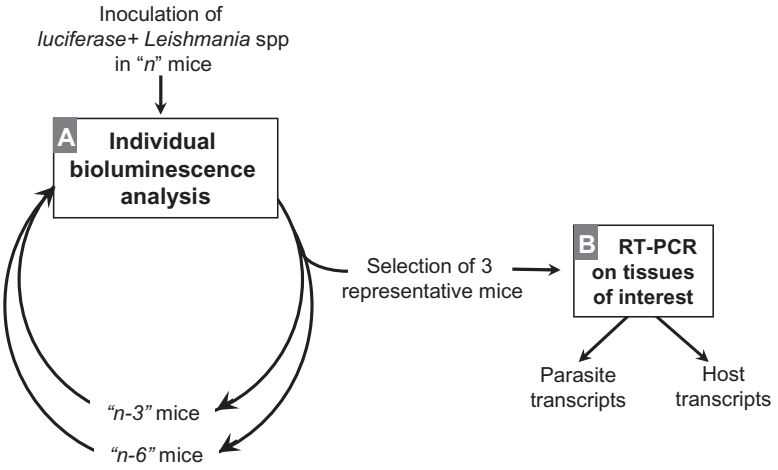

Fig. 1. A two-step procedure for the combined bioluminescence/real-time RT-PCR assay. This multiparametric quantitative approach was performed in two sequential steps.
A. First step: BLI and selection of representative mice. Real-time BLI was performed and three representative mice were selected and sacrificed at different time-points.
B. Second step: mouse transcript abundance by the real-time RT-PCR assay. The tissues of interest (ear and DLN for the C57BL/6/*L. major* model; liver and spleen for the BALB/c/*L. donovani* model) were harvested for the analysis of mouse host transcripts and absolute *Leishmania* amastigote quantification by real-time RT-PCR.

the objectives highlighted above. The main advantages of this approach are: (i) the selection of a limited number of mice with known parasite burden over time post inoculation (PI) with either *L. major* or *L. donovani*; and (ii) the parallel analysis, in real time, of amastigote burden fluctuations and transcriptional signatures displayed by different *Leishmania*-hosting mouse tissues.

Results

Main features of the designed multiparametric approach

Our combined methodology was applied for mice hosting luciferase-expressing *L. major* or *L. donovani*. As outlined in Fig. 1, *n* parasitized mice are imaged for recording *Leishmania* bioluminescence in the tissues of interest, namely the ear for *L. major*-hosting C57BL/6 mice and the liver and the spleen for *L. donovani*-hosting BALB/c mice. At given time-points, three out of *n* mice were selected from these experimental groups on the basis of bioluminescence imaging (BLI) values [similar median BLI values and standard deviations (SDs)] recorded from the above-mentioned tissues (step 1; Fig. 1A). In the second step (Fig. 1B), tissues of interest were harvested from each selected mouse. Then, sampled tissues were processed for total RNA extraction. The abundance of both *Leishmania* and mouse transcripts was then assessed by relative real-time reverse transcription polymerase chain reaction (RT-PCR) using stably expressed reference genes for normalization, samples from unparasitized mice for calibration and spiked *Leishmania* controls as standards for parasite burden quantification (see M and M). Then, the remaining mice ($n - 3$ per group) were kept until the next round of BLI analyses.

The multiparametric approach in a LCL model

Phase delineation and mice selection. Luciferase-expressing *L. major* metacyclic promastigotes (10^4) were inoculated into the ear dermis of C57BL/6 mice ($n = 24$) (Fig. 2). As shown in Fig. 2A, the first cutaneous clinical signs, which were indicated by ear thickness, were noticed only at day 16 PI. This clinical feature was associated to the late development of a macroscopic lesion, as depicted in Fig. 2B1. By contrast, amastigote population size expansion was noted very early in the ear as evidenced by bioluminescence detection (Fig. 2B2). Thus, during the first stage of parasite development no significant correlation was found between the bioluminescence value at the inoculation site and the clinical features. However, the individual follow-up enabled to evidence that high parasite load in the ear (Fig. 2C1) was associated to a larger lesion compared with the mouse ears displaying a lower parasite burden (Fig. 2C2). Thus, the use of BLI was particularly useful for delineating the different phases in mice hosting *L. major* (Fig. 2D). The first phase (day 0 to day 4 PI) corresponded to the bioluminescence background (phase 1, Fig. 2A and C). This phase was followed by a sharp increase of the bioluminescent signal (day 4 to day 29 PI) peaking at day 19 PI (phase 2, Fig. 2B2 and 2C). Interestingly, by day 29, i.e., about 10 days after the *L. major* burden peak, the maximum 'lesion' size was reached (ear thickness around 0.8 mm). The third phase (day 29 to day 47 PI) was characterized by the rapid decrease of the bioluminescence signal to background levels (phase 3, Fig. 2C), whereas the development of the ear "lesion" was still ongoing (Fig. 2A and 2B1). Lastly, the healing phase (day 47 to day 118 PI) was delineated by the absence of BLI signal (phase 4, Fig. 2C), which was coupled with the slow decrease in ear thickness (Fig. 2A). Altogether, the uncoupled dynamics of each recorded parameter are such

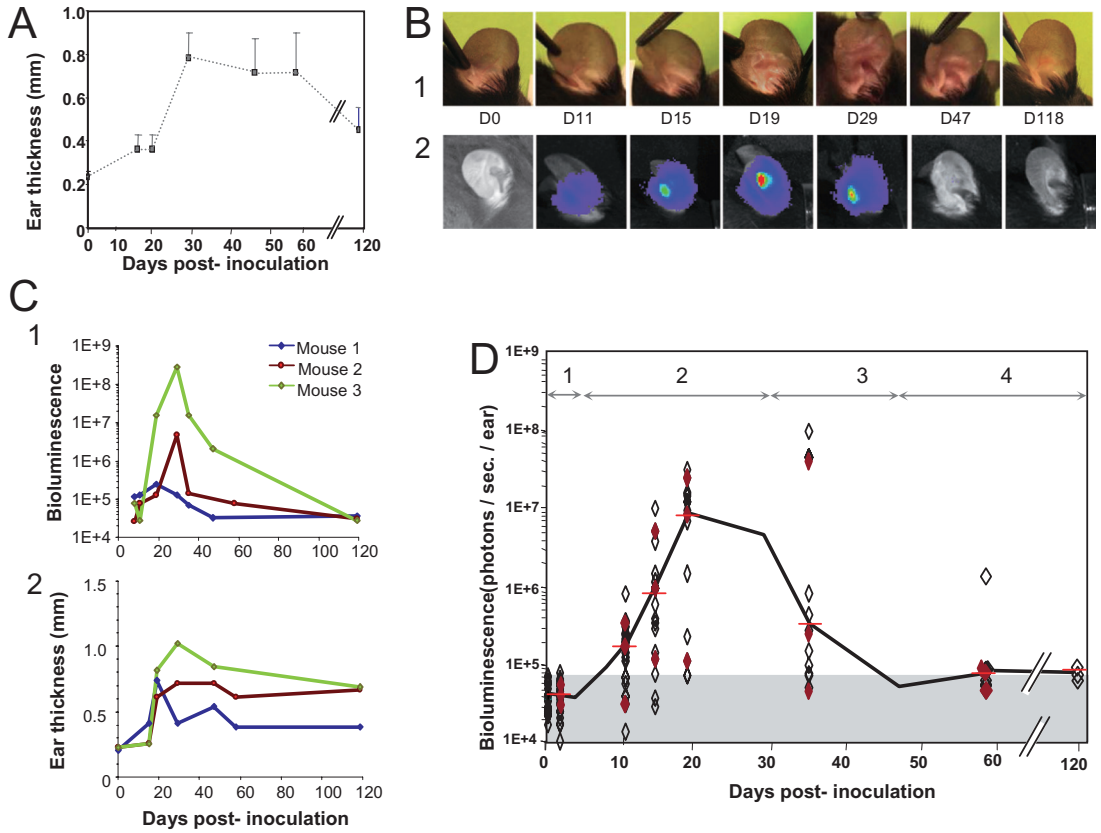

Fig. 2. Monitoring, in parallel, of two *L. major*-driven phenotypic traits and selection of representative C57BL/6 mice. Ten thousand metacyclic promastigotes of luciferase-expressing *L. major* were inoculated into the ear dermis of 24 C57BL/6 mice. Mice were monitored up to 120 days PI.

A. Monitoring of ear thickness displayed at the inoculation site. Medians and SDs are indicated.

B and C. Evolution of ear features (B1) and bioluminescence signals (B2) for a representative mouse. Individual follow-up of bioluminescence (C1) and ear thickness (C2) for three representative mice. These mice displayed high (mouse 1 – blue), moderate (mouse 2 – red) or low (mouse 3 – green) parasite load as determined by bioluminescence signal quantification. Note the different kinetic patterns observed for parasite load (C1) and ear thickness (C2).

D. Bioluminescence analysis at the inoculation site. White lozenges represent individual bioluminescence values. Median values of the entire group are indicated by red bars. The grey area corresponds to the background level of bioluminescence. Four different phases were defined according to parasite load fluctuation (1–4). At each time-point, three representative mice (red lozenges) were sacrificed and processed for real-time PCR experiments.

that there is a need to further explore quantitatively over time the other tissue with which the *Leishmania*-inoculated ear is constantly exchanging information, namely the ear–draining lymph node (DLN). Representative mice selected at each of the four distinct phases (Fig. 2B, red dots) were thus sacrificed for further quantification of mouse and *Leishmania* transcripts in the sampled tissues. This procedure provided important information, especially for the two phases when no BLI signal above the background was detectable.

Recording the abundance of Leishmania *and mouse transcripts in* L. major*-hosting tissues of C57BL/6 mice.* The ears and ear–DLN of selected representative mice were collected at days 4, 11, 15, 19, 35 and 57 PI. Real-time RT-PCR was performed on nucleic acids extracted from these tissues. For each selected mouse, samples were processed to quantify the abundance of *Leishmania* and host transcripts (Fig. 3).

Spiked controls using defined numbers of *L. major* amastigotes were added to unparasitized mouse tissues prior to nucleic acid extraction. Highly reproducible results were obtained for each sample performed in triplicate, and high linearity was maintained over the range of template amastigote numbers added to the tissue (data not shown). The presence of host nucleic acids did not hinder the detection of *Leishmania* transcripts. Under these conditions, the abundance of *L. major* transcripts was analysed simultaneously in the parasites-inoculated ear and the corresponding ear–DLN (Fig. 3A). This analysis provided the missing information for the DLN and for the first and last phases for which there was no

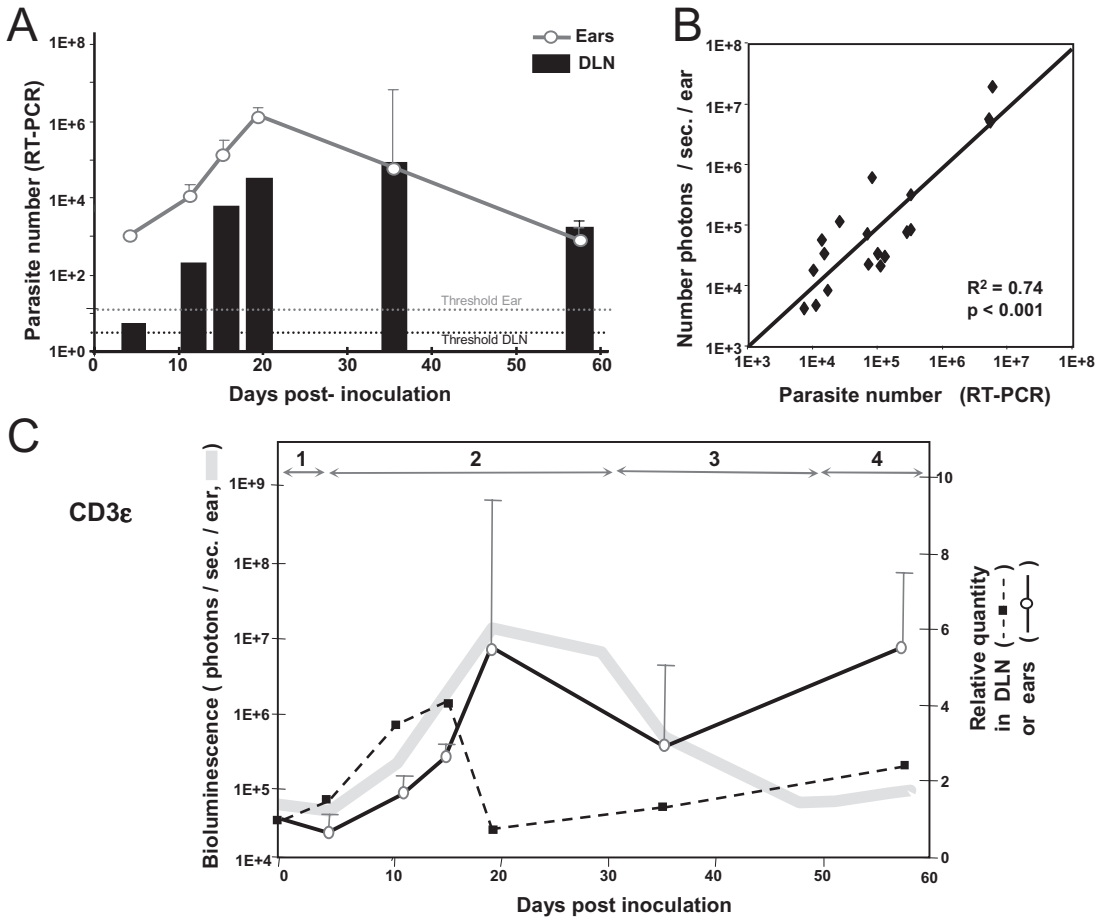

Fig. 3. Monitoring of *L. major* and mouse tissue transcript abundance in the ear and DLN. Ten thousand metacyclic promastigotes of luciferase-expressing *L. major* were inoculated into the ear dermis of 24 C57BL/6 mice. Real-time BLI was performed and three representative mice were selected and sacrificed at different time-points.
A. Quantification of *L. major* mRNA by real-time RT-PCR. *L. major* mRNA was quantified by RT-PCR in ears (grey line) and DLNs (black bars). The sensitivity threshold for the ear and the DLN are indicated by dotted grey and black dotted lines respectively.
B. Correlation between bioluminescence values and amastigote numbers in the ears. Quantification of parasite number was performed by RT-PCR using a standard curve ($n = 19$ ears). Significance and coefficient of determination are indicated. One lozenge represents one ear.
C. Monitoring of CD3ε transcript abundance in ears and DLN. CD3ε transcript abundance in the ear (plain line) and the DLN (dotted line) are shown with parasite load modulation (bioluminescence, thick grey line). Medians and SDs are shown.

BLI value above the background. This real-time RT-PCR assay was five hundred and one hundred times more sensitive than BLI and PCR performed on *Leishmania* DNA (Fig. S1) respectively. An accurate detection of as few as 10 and 4 amastigotes was achieved in the ear and the DLN respectively (0.3–0.4 parasites per mg of tissue). The kinetics of parasite burden in the DLN revealed an expansion between day 11 (300 parasites per DLN) and day 19 (78 000 parasites per DLN). It is noteworthy that there was a strong correlation between the bioluminescence values and the parasite numbers as determined by RT-PCR (Fig. 3B, determination coefficient of 0.74).

To illustrate host transcriptional regulation in mice, the levels of CD3ε transcripts specifically expressed in conventional T lymphocytes were shown in both tissues (Fig. 3C). They remained unchanged in the ear, but they increased slightly in the DLN (1.5-fold increase) during the first phase (background bioluminescence signal). After this, as the parasite load increased at the inoculation site, the CD3ε transcript level reached a peak in the DLN (a fourfold increase) at day 15 PI and was slowly rising in the ear (2.6-fold; Fig. 3B, phase 2). The peak of CD3ε transcript abundance in the ears was observed 4 days later (day 19; 5.6-fold increase) and was associated with a clear decrease in the ear–DLN. During the fourth phase, when the parasite load progressively declined, the level of CD3ε transcripts in both the ear and the DLN remained steady with fold change values oscillating between 2 and 8.

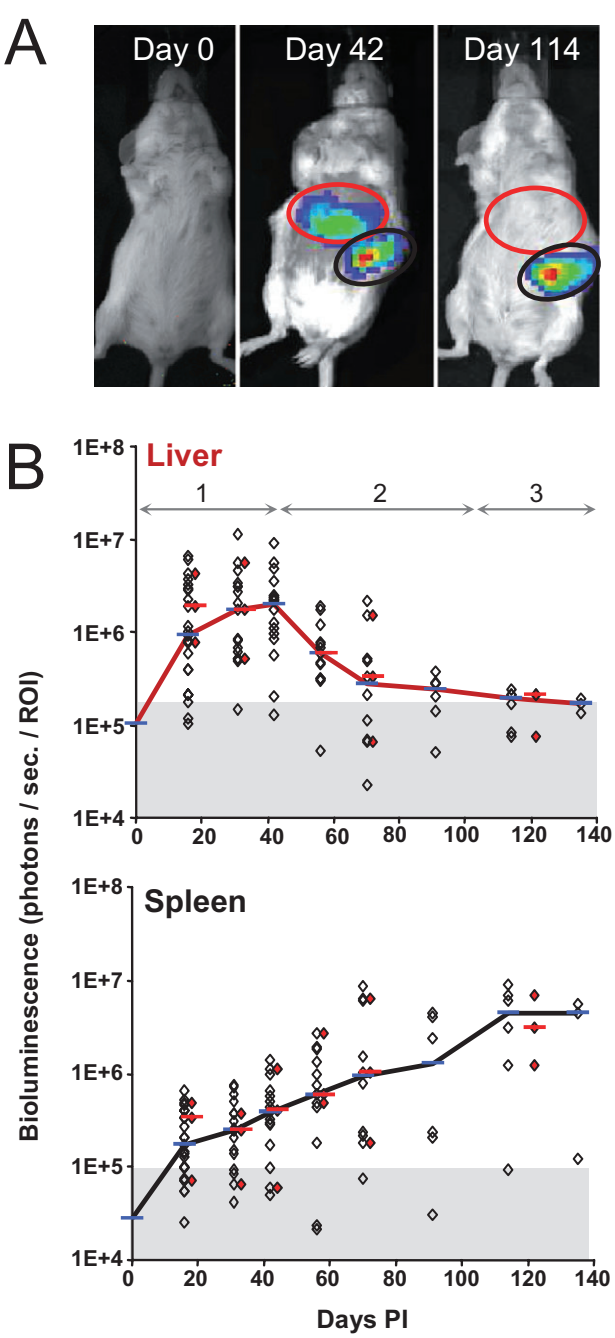

Fig. 4. Monitoring of *L. donovani* bioluminescence in the liver and the spleen and selection of representative BALB/c mice. BALB/c mice ($n = 23$) were inoculated with 5×10^6 promastigotes of luciferase-expressing *L. donovani*.
A. Illustration of bioluminescence signals in a representative mouse. Individual BLI signals were monitored at days 0, 42 and 114 PI in a mouse. The ROI corresponding to the spleen and the liver are displayed in black and red respectively.
B. Bioluminescence monitoring and selection of representative mice. The total photon emission from the liver and the spleen of each mouse is indicated. Median bioluminescence values are displayed for all mice (blue bars) or three selected mice (red bars) at each key time-point. Three different phases were identified from the bioluminescence analysis in the liver. Mice were selected according to liver bioluminescence values at days 16, 31 and 42 and according to spleen bioluminescence values at days 56, 70 and 114 (red lozenges). Grey areas correspond to background bioluminescence signals.

The multiparametric approach in L. donovani*-hosting BALB/c mice*

Phase delineation and mice selection. BALB/c mice were inoculated intraperitoneally with 5×10^6 luciferase-expressing *L. donovani* promastigotes. Liver and spleen BLI for each parasitized mouse was recorded over a period of 140 days to assess the parasite load (Fig 4).

In the liver, the bioluminescence signal rose sharply over the first 20 days PI and then increased slightly to reach a plateau between days 30 and 40. After that and until day 70, BLI values dropped. After this third phase, the bioluminescence signals declined steadily reaching very low levels at 140 days PI.

In the spleen, the development of the parasite population was quite different from that observed in the liver, because BLI values increased gradually and reached a plateau 120 days PI. Of note, this plateau was not due to a saturation phenomenon of the CCD camera. BLI values collected from the liver and the spleen were used to delineate three sequential phases and to select three mice at key time-points according to liver bioluminescence values during phases 1 and 2 and spleen bioluminescence values during phase 3 (Fig. 4B).

Recording the abundance of L. donovani *amastigotes and BALB/c transcripts in the liver and the spleen.* The liver and the spleen of selected mice (see Fig. 1) were processed to determine the abundance of the CXCL1/KC transcript, which codes for a chemokine that is a potent chemotactic factor for neutrophils (Dorman *et al.*, 2005; Kobayashi, 2006), and of the CD68 transcript, which codes for a transmembrane glycoprotein displayed by endosomes of mononuclear phagocytes and dendritic cells (Holness *et al.*, 1993).

The CXCL1 transcript abundance values were distributed along a bell-shaped curve peaking at 31 days PI with a 32-fold increase compared with naïve mice (Fig. 5A1). The CD68 transcript abundance values remained stable from day 0 to day 60 PI (Fig. 5A2) in the spleen. After this, there was a sharp increase until day 122 with fold change values up to 8 in parasitized spleens compared with naïve ones (Fig. 5A2). In both tissues, the parasite burden, as determined by the bioluminescence method, was strictly correlated with either the CXCL1 or the CD68 host transcript abundance (Fig. 5B). To determine the absolute number of *Leishmania* in tissues, parasite transcripts were quantified by real-time RT-PCR. A high linearity was observed over the range of template parasite numbers

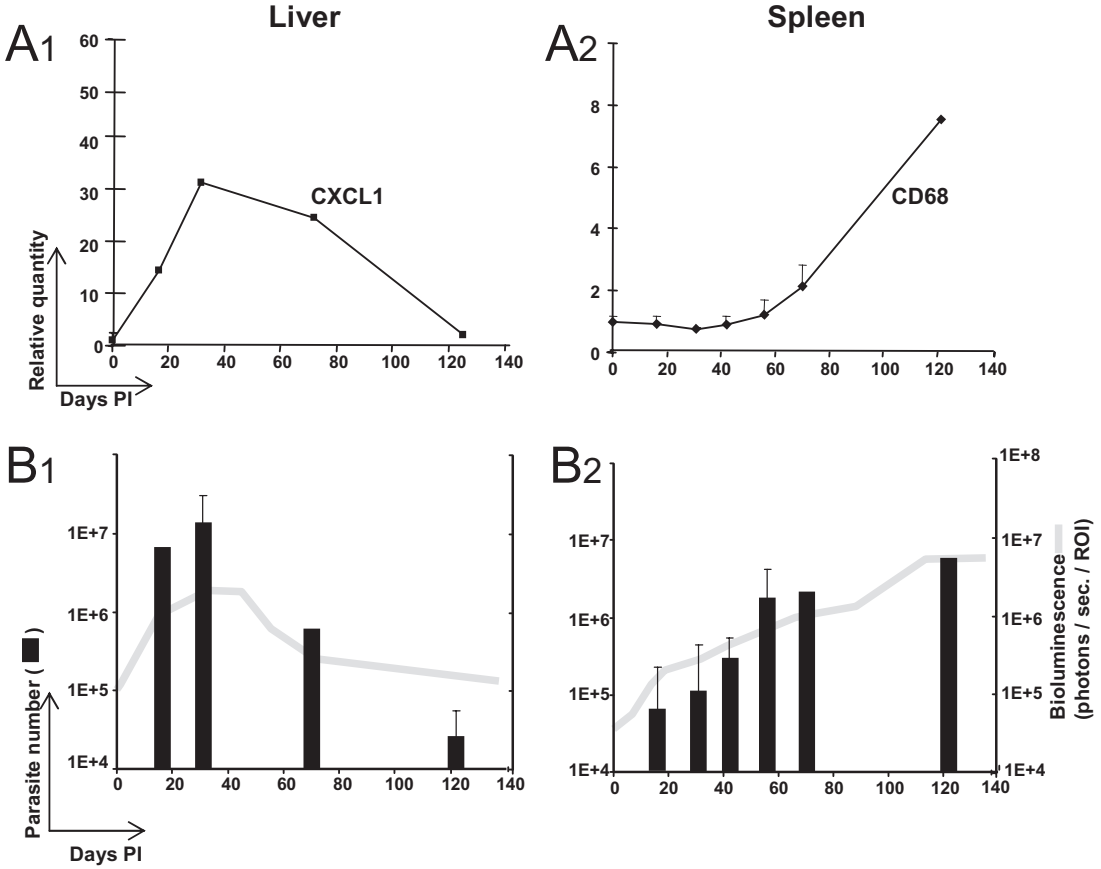

Fig. 5. Real-time RT-PCR analyses in the liver and the spleen of selected *L. donovani*-hosting BALB/c mice. After *L. donovani* inoculation into 23 BALB/c mice, bioluminescence was monitored over 140 days. Three representative mice selected at each time-point were sacrificed (see Fig. 4B). Liver and spleen RNA was extracted, and reverse transcripted and the RT-PCR assay was performed according to *Experimental procedures*. A representative mouse is shown for the liver. Medians and SD obtained for three mice are presented (spleen).
A. Monitoring of mouse transcript abundance in the liver and the spleen. The transcript abundance of CXCL1 and CD68 is shown. Displayed data are the mean fold changes for CXCL1 (A1) and CD68 transcripts (A2).
B. Quantification of *L. donovani* amastigotes. Parasite numbers were determined by real-time RT-PCR in mouse liver (B1) and spleen (B2). The median bioluminescence values are also displayed in parallel (thick grey line). Note the good correlation between the two approaches.
A and B. *In vitro* detection of *L. major* amastigotes by bioluminescence. Different numbers of amastigotes were seeded in each well (A: serial 10-fold dilutions of 10^7 to 10^2 amastigotes; B: 1×10^3 to 5×10^3 parasites) and bioluminescence was measured at 37°C after addition of D-luciferin using the IVIS 100. Medians ± SD are depicted ($n = 3$). The grey area corresponds to background bioluminescence levels. (A) Triplicates were performed for each dilution and bioluminescence values depicted as medians ± 1 SD. The bioluminescent signal was proportional to the parasite number and reached 5×10^7 photons s^{-1} for 1×10^7 parasites per well. (B) Bioluminescence values were obtained from 10 amastigotes-loaded wells and depicted as medians (red bars) and dots. A significant bioluminescence signal (> 1.5×10^4 photons s^{-1} per well) was detected with 1×10^3 parasites per well.
C. *In vivo* detection of amastigotes by bioluminescence. Five thousand luciferase-expressing *L. major* amastigotes were inoculated intradermally into the ears of seven mice. D-luciferin was further inoculated intraperitoneally, and bioluminescence was analysed 25 min later. Values were obtained from the 14 amastigotes-loaded ears and compared with the values of naïve ears. Median values are indicated by red bars. The significance is indicated. The grey area corresponds to background bioluminescence levels.
D. *Ex vivo* threshold of *Leishmania* amastigotes detection by either RT-PCR or by PCR. The minimal number of parasites detectable per ear was determined by real-time RT-PCR (cDNA) and by a DNA-based PCR assay.

added (8 log). The presence of host nucleic acids did not hinder the detection of the *Leishmania* target, even in the presence of very few parasites. Indeed, as few as 10 and 7 parasites could be detected in the liver and the spleen respectively (data not shown). The *L. donovani* transcript abundance and bioluminescence kinetics recorded from the liver and the spleen also had similar profiles, indicating a good correlation between real-time RT-PCR and bioluminescence (Fig. 5B1 and 5B2). However, the PCR assay was more sensitive than the BLI assay; PCR allowed the detection of 24 000 parasites per liver at day 122 PI when bioluminescence was no longer detectable (Fig. 5B1).

Discussion

The present approach extends previous analyses conducted with laboratory mice that have been inoculated

Table 1. Scientific and ethical advantages of the combined bioluminescence/RT-PCR assay.

1. Scientific advantage
   1.1. Bioluminescence related
      - Detection of viable *Leishmania in situ*
      - Selection of representative mice independently of clinical signs (with the preservation of animal heterogeneity)
      - Selection of mice at precise time-points
      - Discarding mice that do not respond properly (mice that remain with negative values of bioluminescence, unresponsive to treatments, etc.)
      - Non-invasive real-time monitoring of parasite load

   1.2. RT-PCR related
      - Analysis on the entire organ/tissue
      - Analysis of a broad spectrum of transcripts (transcripts of the host or the parasite)
      - High sensitivity for parasite load quantification
2. Ethical advantage
      - Sacrifice of a minimal number of mice

The complementary advantages of bioluminescence and RT-PCR are described respectively. The low sensitivity of bioluminescence at low parasite burdens that inhibits detection and quantification parasite load in certain tissues like lymph nodes is 'counterbalanced' by the high sensitivity of RT-PCR.

intradermally with luciferase-expressing *L. major* (Lang *et al*., 2005; 2009; Lecoeur *et al*., 2007; 2010). The combination of BLI with RT-PCR allows correlating, in real time, the amastigote population size fluctuations with the abundance profile of mouse transcripts in each *Leishmania*-hosting tissue collected at different time-points PI.

The key advantages of this combined approach are summarized in Table 1. BLI provides robust and reproducible data for visualizing living amastigotes and allows the selection of a limited number of mice representatives of the whole experimental group for further analysis. Of note, the non-invasive features of BLI limit the number of mice that are sacrificed and thus allow ethical issues to be properly taken into consideration and respected. Moreover, the customized real-time PCR based on the *Leishmania* transcript follow-up described herein enables the detection of very low levels of amastigotes in tissues as distinct as the lymph node, the liver or the spleen. Of note, similar *Leishmania* mRNA levels were found in control tissues spiked with the same number of either promastigotes or amastigotes, which was in agreement with previous studies reporting that the gene expression regulation in *Leishmania* occurs mainly at the translational or post-translational level (Boucher *et al*., 2002; Clayton and Shapira, 2007). In this context, the determination of parasite burden by recording the abundance of transcripts would not be dependent upon the current environment (tissue, cell location) or the *Leishmania* developmental programs. Moreover, the detection of amastigote transcripts paralleled the detection of active transgenic luciferase, thus demonstrating that these transcripts are derived from intact living *Leishmania*. Those results were in agreement with recent *in vivo* and *in vitro* studies in which *Leishmania* nucleic acids detected by PCR came from living parasites and were rapidly degraded following parasite death (Cruz *et al*., 2006; Prina *et al*., 2007). Lastly, the sensitivity of this cDNA-based PCR assay was better than that of several genomic or kinetoplastid DNA assays, thus confirming and extending recent analyses (van der Meide *et al*., 2008a,b; Bretagne *et al*., 2001; Cruz *et al*., 2006; Foulet *et al*., 2007; Prina *et al*., 2007). This increased sensitivity facilitates the monitoring of the discrete modulation of parasite load in tissues that cannot be evidenced solely by BLI. For example, we were able to establish that *L. donovani* amastigotes did persist in the liver.

Furthermore, the application of the strategy described here permitted correlating in real-time mouse tissue transcriptional signatures with the amastigote population size from the onset to the endpoint of the *Leishmania* spp.–mouse interactions. In C57BL/6 mice hosting *L. major*, it was thus possible to estimate the amastigote population size increase that took place during the initial phase before the onset of clinical signs [phase 2; Fig. 2C (Belkaid *et al*., 2000)] and to characterize the CD3ε transcript expression kinetic profile in the ear–DLN with which the ear is constantly exchanging information (Debes *et al*., 2005; Tomura *et al*., 2008).The present combined assay will also be relevant for dissecting factors and mechanisms of drug resistance during chemotherapy. As previously shown by Lecoeur *et al*. (2007), a too short duration of topical ointment application on *L. major*-hosting ears may lead to parasite load rebound, because this latter phenotype is uncoupled from any clinically detectable damage of the ear (Lecoeur *et al*., 2007). In this context, the analysis of immune transcript abundance in both the ear and the ear–DLN of these mice, selected on bioluminescence values, will assist in the characterization of mechanisms that control the parasite- and mouse-driven processes that allow *Leishmania* to complete its full developmental program from its early establishment to its persistence.

Future experiments, with the use of sand flies hosting *L. donovani* or *L. chagasi* metacyclic promastigotes, will be able to characterize each step of the processes that allow these *Leishmania* species to proceed from the dermis to the liver, bone marrow and spleen. In addition to CXCL1 and CD68, which were selected to illustrate contrasting outcomes in the liver and the spleen, many other transcriptional signatures can be simultaneously and quantitatively monitored for each mouse tissue and evaluated for correlations with amastigote burdens.

Because of its numerous advantages and, in particular, the high number of transcript profiles that can be performed in the same sample (Table 1), the present combined assay will lead to fully integrated studies that can

accelerate the development of novel and relevant therapeutic vaccine approaches and anti-parasitic strategies. The current development of new bioluminescent reporter molecules (Lang *et al*., 2009), mouse strains expressing relevant bioluminescent probes (Contag, 2008) and a more sensitive CCD camera in BLI will help to describe the dynamic and renewed reciprocal communications between the *Leishmania* parasite and its mammal host at the tissue, cellular and subcellular levels.

Experimental procedures

Mice

Six-week-old female Swiss nu/nu, BALB/c and C57BL/6 mice were purchased from Charles River (Saint Germain-sur-l'Arbresle, France) and were maintained under specific pathogen-free conditions at the Pasteur Institute in compliance with European animal welfare standards.

Parasites

Leishmania major strain NIH 173 (MHOM/IR/-/173) and *L. donovani* (*LD1S*/MHOM/SD/00-strain 1S) were used in this study. Transfection of *Leishmania* parasites to express the firefly luciferase was performed as previously described (Lang *et al*., 2005; Lecoeur *et al*., 2007). Briefly, the *luciferase* coding region was cloned into the *Leishmania* expression vector pF4X1.HYG (Jenabioscience, Jena, Germany). Following transfection and electroporation, transfected *Leishmania* promastigotes were selected on semi-solid media containing 100 μg ml^{-1} of hygromycin B (Goyard *et al*., 2003).

Mouse experimental models

Localized cutaneous leishmaniasis model. Transgenic luciferase-expressing *L. major* amastigotes were isolated from parasitized Swiss nude mice inoculated 2 months before under a BSL-2 cabinet (Lang *et al*., 2005). After the initial amastigote differentiation into promastigote, parasites were grown at 26°C in supplemented M199 medium as previously described (Goyard *et al*., 2003). Metacyclic promastigotes were isolated from 6 days stationary phase cultures using a discontinuous density gradient (Späth and Beverley, 2001).

C57BL/6 mice were anaesthetized by intraperitoneal administration of a Ketamine (120 mg kg^{-1} Imalgene 1000, Merial, France) and Xylasine (4 mg kg^{-1}; Rompun 2%, Bayer, Leverkusen, Germany) mixture. Ten thousand metacyclic promastigotes in 10 μl of Dulbecco's phosphate buffered saline (PBS) were injected into the right ear dermis. Each mouse was tagged in the contralateral left ear for kinetic experiments. Ear thickness was measured using a direct reading Vernier caliper (Thomas Scientific, Swedesboro, NJ).

Visceral leishmaniasis model. Transgenic luciferase-expressing *L. donovani* amastigotes were isolated from the liver of a BALB/c mouse inoculated 6 months before with stationary phase promastigotes. The liver was cut in small pieces and dissociated on a 70 μm cell strainer (BD Falcon) in supplemented M199 medium. The homogenate was placed at 26°C to allow promastigote growth. After 1 week, promastigotes were seeded at a concentration of 1×10^5 parasites per ml for 9 days. Five million stationary phase promastigotes in 200 μl of PBS were inoculated intraperitoneally in anaesthetized mice. Ear punching was used for individual mouse identification and follow-up.

In vitro *bioluminescence imaging assay of* L. major *amastigotes*

Amastigotes were isolated from the footpads of transgenic *L. major*-parasitized nude mice. Different parasite numbers (10^2, 10^3, 5×10^3, 10^4, 5×10^4, 10^5, 10^6 and 10^7) were suspended in 100 μl PBS–Ca^{2+}–Mg^{2+}, in black 96-well microplates (Microfluor®, Dynatech Laboratories, Chantilly, France). Luciferin (D-Luciferin potassium salt, Xenogen, CA), i.e. the luciferase substrate, was added to each well at a final concentration of 0.6 μg ml^{-1}. Bioluminescence signals were acquired 15 min later in the imaging chamber of the IVIS™ Imaging System 100 Series.

In vivo *bioluminescence imaging assay at the tissue/organ level*

At different time-points following *Leishmania* inoculation, luciferin was injected intraperitoneally at 150 and 300 mg kg^{-1} for the LCL and VL models respectively. Mice were anaesthetized in a 2.5% isoflurane atmosphere (Aerane®, Baxter SA, Maurepas, France) for 5 min and placed in the imaging chamber of the IVIS™ Imaging System 100 Series (Xenogen). Acquisition of emitted photons with a charge-coupled device camera was performed 25 min (LCL model) or 10 min (VL model) following intraperitoneal luciferin inoculation in the previously defined region of interest (ROI) that delimited the surface of the entire tissue or organ to analyse. The same ROI was applied to every mouse at every time-point. Total photon emission was expressed in photons/s/ROI and median bioluminescence values and SDs were calculated for each LCL and VL experimental model group.

Mouse distribution within groups on the basis of median bioluminescence values

At designated time-points PI, a group of three representative mice, i.e. presenting median bioluminescence and SD values similar to the whole corresponding group, were sacrificed for host gene expression analysis by real-time PCR. Control, naïve mice were analysed in parallel.

Tissue removal for RNA or DNA extraction

At different time-points PI, three mice were selected and sacrificed. Tissues and organs were removed and fragmented using either the Precellys 24 System (ears, lymph nodes and spleens) or the Ultra Turrax polytron (livers) (see Table 2). RNA isolation was performed with the RNeasy Plus Mini kit (Qiagen, Courtaboeuf, France), according to the manufacturer's instructions. Evaluation of RNA quality was performed by optical density

Table 2. Overview of RNA extraction from different tissues of interest and RT-PCR analysis.

	Tissues			
	Liver	Spleen	Ear	Peripheral lymph node
1. Entire tissue handling				
• Tissue weight (mg)	1000–1600	100–400	20–200	2–30
• Lysis buffer (ml)	5	1	1	0.4
• Lyser/homogenizer	Ultra Turrax®	Precellys®24	Precellys®24	Precellys®24
• Final volume of the homogenate (ml)	4.8	1	1	0.4
2. Column-based RNA extraction				
• initial volume (µl)	250	250	250	400
• RNA yield (µg)	0.6–3	10–40	2–15	1–40
3. Real-time PCR				
• Number of PCR per organ	1400–6000	4000–14 800	800–6000	100–3700

At different time-points PI, samples were collected and fragmented in Qiagen lysis buffer as described (1). Information of interest including the weight, lysis buffer volume, RNA yield (2) and total theoretical number of PCR per organ are listed (3). The numbers indicate the minimum and maximum values of the corresponding data.

measurement using the Nanodrop (ThermoFisher Scientific) (Schroeder *et al.*, 2006).

Cell lysis and DNA isolation from tissues or from lesion-derived purified amastigotes were performed with the DNeasy Tissue kit (Qiagen) (Prina *et al.*, 2007) according to the manufacturer's instructions.

Transcriptional analyses by real-time RT-PCR

Total RNAs were reverse transcribed to first strand cDNA using random hexamers (Roche Diagnostics) and Moloney Murine Leukemia Virus Reverse Transcriptase (Invitrogen, Life Technologies). PCR were performed in a final volume of 10 µl per reaction in white ultraAmp 384-well PCR plates (Sorenson, Bioscience, Salt Lake City, UT, USA) using a LightCycler® 480 system (Roche Diagnostics, Meylan, France). Briefly, 1 µl of sample (DNA or cDNA) was added to 9 µl of a master mix containing 5 µl of QuantiTect SYBR Green Kit (Qiagen) and 4 µl of nuclease-free water with primers (Guaranteed Oligos™, Sigma-Aldrich) at a final concentration of 0.5 µM. Activation of the Qiagen *Thermophilus aquaticus* polymerase was performed at 95°C for 15 min. The PCR program included 40 cycles of denaturation at 95°C for 10 s, annealing at 54°C for 25 s and extension at 72°C for 30 s. SYBR Green fluorescent emission was measured at the end of the elongation step. Subsequently, a melting curve program was applied with a continuous fluorescent measurement starting at 70 C and ending at 95 C (ramping rate of 0.1°C s^{-1}). Crossing point values (Cp) were determined by the second derivative maximum method of the LightCycler® 480 Basic Software. Raw Cp values were used as input for qBase, a flexible and open source program for qPCR data management and analysis (Hellemans *et al.*, 2007). For normalization calculations, candidate control genes were tested – *pgk1* (phosphoglycerate kinase 1), *h6pd* (hexose 6-phosphate dehydrogenase), *ldha* (lactate dehydrogenase), *nono* (non-POU domain-containing octamer binding protein), *g6pd* (glucose 6-phosphate deshydrogenase), *hprt* (hypoxanthine–guanine phosphoribosyltransferase), *tbp* (TATAA–box binding protein), *l19* (ribosomal protein L19), *gapdh* (glyceraldehyde 3-phosphate dehydrogenase), *rpIIe* (RNA Pol E) and *ywhaz* (tyrosine 3/tryptophan 5–monooxygenase activation protein, zeta polypeptide) – with the geNorm (Vandesompele *et al.*, 2002) and Normfinder programs (Andersen *et al.*, 2004). *G6pd* and *h6pd* were selected as the most stable reference genes for the ears and the lymph nodes of C57Bl/6 mice. *rpIIe* and *tbp* were selected for the BALB/c spleens and *l19* and *ldha* for BALB/c livers. More details about the reference gene selection procedure can be found in Fig. S2.

Experimental procedure for quantifying Leishmania *in tissues/organs*

Serial 10-fold dilutions of parasites (from 10^8 to 10^1) were added to either ears or ear–DLN recovered from C57BL/6 naïve mice (LCL model) or to livers or spleens recovered from BALB/c naïve mice (VL model). Total RNAs were further extracted and processed for real-time RT-PCR as described above. The *Leishmania* gene target (*ssrRNA*) was selected for quantifying the number of parasites. Two mouse reference genes (see above) were used for normalization calculations. A linear regression for each standard curve was determined (quantification of *Leishmania* parasites against the relative expression of *ssrRNA* values). The *P*-value of the linear correlation between bioluminescence values and real-time RT-PCR values for the quantification of parasites was determined in the statistical environment R.

Acknowledgements

The authors are very grateful to Christine Maillet for her excellent technical assistance and Thierry Angelique for his help in taking care of our mice.

This work was supported by grants from i) Région Ile de France ii) the Institut Pasteur and iii) the Fonds Dédié Sanofi-Aventis/Ministère de l'Enseignement Supérieur et de la Recherche "Combattre les Maladies Parasitaires".

References

Alexander, J., Carter, K.C., Al-Fasi, N., Satoskar, A., and Brombacher, F. (2000) Endogenous IL-4 is necessary for effective drug therapy against visceral leishmaniasis. *Eur J Immunol* **30:** 2935–2943.

Andersen, C.L., Jensen, J.L., and Orntoft, T.F. (2004) Normalization of real-time quantitative reverse transcription-PCR data: a model-based variance estimation approach to identify genes suited for normalization, applied to bladder and colon cancer data sets. *Cancer Res* **64:** 5245–5250.

Banuls, A.L., Hide, M., and Prugnolle, F. (2007) *Leishmania* and the leishmaniases: a parasite genetic update and advances in taxonomy, epidemiology and pathogenicity in humans. *Adv Parasitol* **64:** 1–109.

Belkaid, Y., Mendez, S., Lira, R., Kadambi, N., Milon, G., and Sacks, D. (2000) A natural model of *Leishmania major* infection reveals a prolonged 'silent' phase of parasite amplification in the skin before the onset of lesion formation and immunity. *J Immunol* **165:** 969–977.

Belkaid, Y., Von Stebut, E., Mendez, S., Lira, R., Caler, E., Bertholet, S., *et al*. (2002) CD8(+) T cells are required for primary immunity in C57BL/6 mice following low-dose, intradermal challenge with *Leishmania major*. *J Immunol* **168:** 3992–4000.

Boucher, N., Wu, Y., Dumas, C., Dube, M., Sereno, D., Breton, M., and Papadopoulou, B. (2002) A common mechanism of stage-regulated gene expression in *Leishmania* mediated by a conserved 3′-untranslated region element. *J Biol Chem* **277:** 19511–19520.

Bretagne, S., Durand, R., Olivi, M., Garin, J.F., Sulahian, A., Rivollet, D., *et al*. (2001) Real-time PCR as a new tool for quantifying *Leishmania* infantum in liver in infected mice. *Clin Diagn Lab Immunol* **8:** 828–831.

Clayton, C., and Shapira, M. (2007) Post-transcriptional regulation of gene expression in trypanosomes and leishmanias. *Mol Biochem Parasitol* **156:** 93–101.

Contag, P.R. (2008) Bioluminescence imaging to evaluate infections and host response *in vivo*. *Methods Mol Biol* **415:** 101–118.

Cruz, I., Chicharro, C., Nieto, J., Bailo, B., Canavate, C., Figueras, M.C., and Alvar, J. (2006) Comparison of new diagnostic tools for management of pediatric Mediterranean visceral leishmaniasis. *J Clin Microbiol* **44:** 2343–2347.

Debes, G.F., Arnold, C.N., Young, A.J., Krautwald, S., Lipp, M., Hay, J.B., and Butcher, E.C. (2005) Chemokine receptor CCR7 required for T lymphocyte exit from peripheral tissues. *Nat Immunol* **6:** 889–894.

Dorman, R.B., Gujral, J.S., Bajt, M.L., Farhood, A., and Jaeschke, H. (2005) Generation and functional significance of CXC chemokines for neutrophil-induced liver injury during endotoxemia. *Am J Physiol Gastrointest Liver Physiol* **288:** G880–G886.

Foulet, F., Botterel, F., Buffet, P., Morizot, G., Rivollet, D., Deniau, M., *et al*. (2007) Detection and identification of *Leishmania* species from clinical specimens by using a real-time PCR assay and sequencing of the cytochrome B gene. *J Clin Microbiol* **45:** 2110–2115.

Goyard, S., Segawa, H., Gordon, J., Showalter, M., Duncan, R., Turco, S.J., and Beverley, S.M. (2003) An *in vitro* system for developmental and genetic studies of *Leishmania donovani* phosphoglycans. *Mol Biochem Parasitol* **130:** 31–42.

Hellemans, J., Mortier, G., De Paepe, A., Speleman, F., and Vandesompele, J. (2007) qBase relative quantification framework and software for management and automated analysis of real-time quantitative PCR data. *Genome Biol* **8:** R19.

Holness, C.L., Silva, R.P., Fawcett, J., Gordon, S., and Simmons, D.L. (1993) Macrosialin, a mouse macrophage-restricted glycoprotein, is a member of the lamp/lgp family. *J Biol Chem* **268:** 9661–9666.

Kaye, P.M., Svensson, M., Ato, M., Maroof, A., Polley, R., Stager, S., *et al*. (2004) The immunopathology of experimental visceral leishmaniasis. *Immunol Rev* **201:** 239–253.

Kimblin, N., Peters, N., Debrabant, A., Secundino, N., Egen, J., Lawyer, P., *et al*. (2008) Quantification of the infectious dose of *Leishmania major* transmitted to the skin by single sand flies. *Proc Natl Acad Sci USA* **105:** 10125–10130.

Kobayashi, Y. (2006) Neutrophil infiltration and chemokines. *Crit Rev Immunol* **26:** 307–316.

Lang, T., Goyard, S., Lebastard, M., and Milon, G. (2005) Bioluminescent *Leishmania* expressing luciferase for rapid and high throughput screening of drugs acting on amastigote-harbouring macrophages and for quantitative real-time monitoring of parasitism features in living mice. *Cell Microbiol* **7:** 383–392.

Lang, T., Lecoeur, H., and Prina, E. (2009) Imaging *Leishmania* development in their host cells. *Trends Parasitol* **25:** 464–473.

Lecoeur, H., Buffet, P., Morizot, G., Goyard, S., Guigon, G., Milon, G., and Lang, T. (2007) Optimization of topical therapy for *Leishmania major* localized cutaneous leishmaniasis using a reliable C57BL/6 model. *PLoS Negl Trop Dis* **1:** e34.

Lecoeur, H., Buffet, P.A., Milon, G., and Lang, T. (2010) Early curative applications of the aminoglycoside WR279396 on an experimental *Leishmania major*-loaded cutaneous site do not impair the acquisition of immunity. *Antimicrob Agents Chemother* **54:** 984–990.

van der Meide, W., Guerra, J., Schoone, G., Farenhorst, M., Coelho, L., Faber, W., *et al*. (2008a) Comparison between quantitative nucleic acid sequence-based amplification, real-time reverse transcriptase PCR, and real-time PCR for quantification of *Leishmania* parasites. *J Clin Microbiol* **46:** 73–78.

van der Meide, W.F., Peekel, I., van Thiel, P.P., Schallig, H.D., de Vries, H.J., Zeegelaar, J.E., and Faber, W.R. (2008b) Treatment assessment by monitoring parasite load in skin biopsies from patients with cutaneous leishmaniasis, using quantitative nucleic acid sequence-based amplification. *Clin Exp Dermatol* **33:** 394–399.

Murphy, M.L., Cotterell, S.E., Gorak, P.M., Engwerda, C.R., and Kaye, P.M. (1998) Blockade of CTLA-4 enhances host resistance to the intracellular pathogen, *Leishmania donovani*. *J Immunol* **161:** 4153–4160.

Murray, H.W., Berman, J.D., Davies, C.R., and Saravia, N.G. (2005) Advances in leishmaniasis. *Lancet* **366:** 1561–1577.

Nicolas, L., Prina, E., Lang, T., and Milon, G. (2002) Real-time PCR for detection and quantitation of leishmania in mouse tissues. *J Clin Microbiol* **40:** 1666–1669.

Peters, N.C., Egen, J.G., Secundino, N., Debrabant, A., Kimblin, N., Kamhawi, S., *et al*. (2008) *In vivo* imaging reveals an essential role for neutrophils in leishmaniasis transmitted by sand flies. *Science* **321:** 970–974.

Prina, E., Roux, E., Mattei, D., and Milon, G. (2007) *Leishmania* DNA is rapidly degraded following parasite death: an analysis by microscopy and real-time PCR. *Microbes Infect* **9:** 1307–1315.

Sacks, D., and Noben-Trauth, N. (2002) The immunology of susceptibility and resistance to *Leishmania major* in mice. *Nat Rev Immunol* **2:** 845–858.

Sakthianandeswaren, A., Foote, S.J., and Handman, E. (2009) The role of host genetics in leishmaniasis. *Trends Parasitol* **25:** 383–391.

Schroeder, A., Mueller, O., Stocker, S., Salowsky, R., Leiber, M., Gassmann, M., *et al.* (2006) The RIN: an RNA integrity number for assigning integrity values to RNA measurements. *BMC Mol Biol* **7:** 3.

Scott, P. (2005) Immunologic memory in cutaneous leishmaniasis. *Cell Microbiol* **7:** 1707–1713.

Späth, G.F., and Beverley, S.M. (2001) A lipophosphoglycan-independent method for isolation of infective *Leishmania* metacyclic promastigotes by density gradient centrifugation. *Exp Parasitol* **99:** 97–103.

Tomura, M., Yoshida, N., Tanaka, J., Karasawa, S., Miwa, Y., Miyawaki, A., and Kanagawa, O. (2008) Monitoring cellular movement *in vivo* with photoconvertible fluorescence protein 'Kaede' transgenic mice. *Proc Natl Acad Sci USA* **105:** 10871–10876.

Vandesompele, J., De Preter, K., Pattyn, F., Poppe, B., Van Roy, N., De Paepe, A., and Speleman, F. (2002) Accurate normalization of real-time quantitative RT-PCR data by geometric averaging of multiple internal control genes. *Genome Biol* **3:** RESEARCH0034.

Supporting information

Additional Supporting Information may be found in the online version of this article:

Fig. S1. Sensitivity of RT-PCR and bioluminescence assays for the detection of luciferase-expressing *L. major* amastigotes.
A–B) *In vitro* detection of *L. major* amastigotes by bioluminescence.
Different numbers of amastigotes were seeded in each well (A: serial 10-fold dilutions of 10^7 to 10^2 amastigotes B: 1×10^3 to 5×10^3 parasites) and bioluminescence was measured at 37°C after addition of D-luciferin using the IVIS 100. Medians +/– SD are depicted (n = 3). The grey area corresponds to background bioluminescence levels.
(A) Triplicates were performed for each dilution and bioluminescence values depicted as medians +/– 1SD. The bioluminescent signal was proportional to the parasite number and reached 5×10^7 photons/sec for 1×10^7 parasites per well (B) Bioluminescence values were obtained from 10 amastigotes-loaded wells and depicted as medians (red bars) and dots. A significant bioluminescence signal ($> 1.5 \times 10^4$ photons/sec/well) was detected with 1×10^3 parasites per well.
C) *In vivo* detection of amastigotes by bioluminescence.
Five thousand luciferase-expressing *L. major* amastigotes were inoculated intradermally into the ears of 7 mice. D-luciferin was further inoculated intraperitoneally, and bioluminescence was analyzed 25 min later. Values were obtained from the 14 amastigotes-loaded ears and compared to the values of naïve ears. Median values are indicated by red bars. The significance is indicated. The grey area corresponds to background bioluminescence levels.
D) *Ex vivo* threshold of *Leishmania* amastigotes detection by either RT-PCR or by PCR.
The minimal number of parasites detectable per ear was determined by real time RT-PCR (cDNA) and by a DNA-based PCR assay.

Fig. S2. Average expression stability values of control genes for the BALB/c spleens.
The geNorm applet calculates the gene-stability measure M, which is an average pairwise variation of a particular gene with all other control genes tested. Expression stability is plotted for each of the candidate reference genes, progressing from the least stable genes with a higher M value to the most stable genes with a lower M value. For the spleen samples in this experimental system, the two most stable genes were RPIIe and TBP.